

Pile-oscillation results for stainless steel with local and 3D global measurements

Thomas Ligonnet^{1,*}, Axel Laureau², Oskari Pakari^{1,3}, Daniel Clément¹, Alexis Dupont-Bembinoff¹, Gilles Noguère⁴, Andreas Pautz^{1,3}, and Vincent Lamirand^{1,3}

¹EPFL, Switzerland

²CNRS Grenoble, France

³PSI, Switzerland

⁴CEA, France

(*) thomas.ligonnet@epfl.ch

Abstract— The BLOOM pile-oscillation program on stainless steel and minor alloying elements was successfully conducted in the CROCUS reactor at EPFL between fall 2024 and spring 2025. For this purpose, a pile-oscillator and a new instrumented channel capable of measuring thermal neutrons as close as 2 mm from the sample were developed in-house, thanks to the previous development in miniature neutron scintillators. Furthermore, the SAFFRON detector array, consisting of 160 such miniature detectors, was used to measure the neutron flux across the core and within the instrumented channel. Using SAFFRON, it was verified that the chosen oscillation location was suitable and point kinetics could be applied, as the induced perturbation did not cause globalized flux redistributions. Local perturbations were measurable up to 15 cm from the sample, setting the minimum distance beyond which the global perturbation was measurable. A total of 45 pile-oscillations were performed, including measurements of 40 different samples and five repetitions of a gold sample at different points of the campaign. For each experiment, the amplitudes of the local and global perturbations and the corresponding reactivity worth were successfully measured, with relative uncertainties as low as 0.07% for the heaviest samples local perturbation, and uncertainty on reactivity worths of 0.04 pcm. Future developments will include the addition of new samples and references such as the D₂O. Further developments are also planned to be able to perform pile-oscillations at higher power.

Keywords — Pile-Oscillation, CROCUS, Experiments, zero-power reactor, Cross-Section.

I. INTRODUCTION

THE BLOOM experimental program consists of pile-oscillation experiments conducted in the CROCUS zero-power reactor of the LRS at EPFL. The BLOOM program is part of LRS's broader initiative, the HARVEST-X project, which aims to produce new constraints for stainless-steel nuclear data evaluations through integral experimental results [1,2]. Within this context, BLOOM was developed to reproduce and extend the critical experiments conducted as part of the CEA-EPFL PETALE program, the other part being dedicated to transmission [3,4]. Specifically, samples directly extracted from spare reflectors used in the PETALE program were

oscillated during the experimental campaign.

Pile-oscillation experiments involve repeatedly inserting and extracting samples into a nuclear reactor to periodically perturb its state [5]. Although the principle is not new, pile-oscillation experiments have regained interest because they enable lower uncertainties and a higher versatility compared to traditional critical experiments [6–8]. Furthermore, the CEA MAESTRO program demonstrated the feasibility of hybrid pile-oscillation experiments, in which both localized and generalized effects of the oscillated sample are measured. The MAESTRO program also validated the equivalence between the open-loop method, which allows reactor power to drift during measurements, and the traditional closed-loop method, in which reactivity effects are actively compensated [9,10]. BLOOM is among the experimental programs inspired by these results, and its primary experimental campaign was conducted between fall 2024 and spring 2025.

This project is the latest in the series of modulation experimental programs that takes place in the CROCUS reactor. It takes full advantage of the developments and insight gained from the previous fuel rod oscillator COLIBRI and for the rotating oscillator PISTIL [2,11,12].

In the first part of this study, the adequacy of our oscillator and detector location is verified using the EPFL miniature scintillators distributed in core in the SAFFRON detector array [13,14], ensuring that oscillation does not induce global flux redistribution. Subsequently, an instrumented channel, newly developed to measure localized effects at an unprecedented proximity, is employed. Using this channel, nine miniature detectors of SAFFRON measure the local effects of the samples at a distance of 2 mm from their surfaces, thus maximizing both the amplitude and precision of the local perturbations' measurements. Finally, the data are processed using state-of-the-art methodologies, applicable to pile-oscillation and modulation experiments, including developments performed for the CORTEX program [15,16]. The experiment with the gold reference sample was repeated five times at different intervals from the beginning to the end of the program, verifying the consistency of the experimental setup and methodologies throughout the study. In total, 45 measurements were conducted on 40 distinct samples and 25 materials, providing an extensive dataset covering both local and global

core perturbations, as well as reactivity worths. Results that are of interest for current and future nuclear data validations and assimilations [17,18].

II. SETUP AND METHODOLOGY

A. The CROCUS Reactor

The CROCUS reactor is a zero-power research reactor located in Lausanne, Switzerland. It is a light-water pool type reactor consisting of two concentric fuel zones with low enrichment. The inner zone comprises 336 fuel rods containing uranium oxide pellets enriched to 1.806 wt.%, while the outer zone is currently composed of 180 fuel rods of metallic uranium and is enriched at 0.947 wt.%. The number of rods in this outer zone can vary depending on the experimental campaign, in this instance 4 additional rods with respect to the standard configuration compensate for the reactivity worth of the SAFFRON detector array. The reactor operates at ambient pressure and a controlled temperature of 20 °C. The maximum power authorized by its operating license is 100 W, resulting in a maximum neutron flux of $2.5 \times 10^9 \text{ cm}^{-2} \cdot \text{s}^{-1}$ at the core center [19,20].

The primary reactivity control mechanism of CROCUS is a spillway that regulates the reactor's water level. Its height can be adjusted with a resolution of 0.1 mm, resulting in a reactivity uncertainty of 0.4 pcm. In its typical configuration, two additional boron carbide absorber rods can also be employed to control its criticality. These rods have an insertion calibration precision of 1 mm, corresponding to an average reactivity control precision of 0.2 pcm. The reactor's permanent power monitoring system consists of two boron-coated compensated ionization chambers and two fission chambers, the last two also function as the safety monitors.

In the BLOOM experimental configuration, the northern absorber rod is removed and replaced with an instrumented oscillation channel. Four Photonis CFUL-01 fission chambers are positioned at each cardinal direction and added to the permanent instrumentation to enhance neutron counting capabilities during oscillations, and provide references in comparison with previous noise and modulation campaigns [11,21].

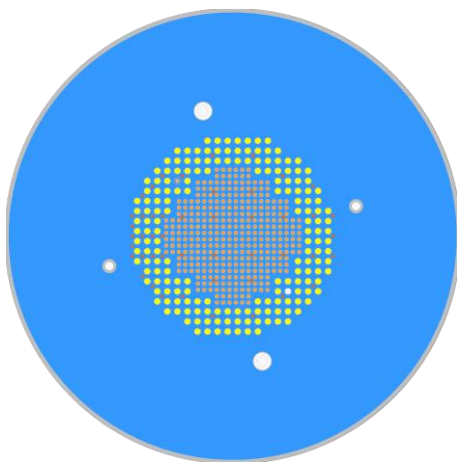


Fig. 1. Axial cut at mid-height of the core of the Serpent2 model of the CROCUS reactor. In this model the size of SAFFRON scintillators (orange squares) is magnified by a factor ten for visibility, with the exception of the ones in the instrument channel, which are visible in a separate close-up (Fig. 4).

B. The SAFFRON Detector Array

SAFFRON is an array composed of 160 miniature LiF:ZnS neutron scintillation detectors, or MiMi detectors [22]. The scintillators are coupled with optical fibers to SiPMs, which are periodically read, and each neutron detection is treated individually using a time tagging system. Of the 160 detectors, 149 are set at fixed positions within the reactor core. Most detectors are arranged in three axial layers at heights of 25, 50, and 75 cm, named L1, L2, and L3 respectively, while a few additional detectors are positioned at intermediate layers LM1 and LM2 close to control rod guide tubes. The detectors are distributed throughout the core cross-section, as shown in Fig. 1, to allow for flux map measurements. The remaining 11 fibers can be freely repositioned within the core; currently, nine of these detectors are employed in the instrumented experimental channel [13,14].

C. Instrumented Experimental Channel

The instrumented experimental channel consists of two components: the pile-oscillator and the in-air instrumented channel. A picture of the installed experimental setup is shown in Fig. 2. The pile-oscillator, referred to as POLLEN, consists of a brushless motor coupled to a wheel around which a wire is wound, allowing a displacement precision of 0.25 mm (on the left in the figure). Detailed descriptions of the motor, along with its associated software and hardware, are available in the proceedings of the previous conference edition [23]. On the right, the wire is attached to an aluminum ruler, which maintains sample alignment within the channel via the channel's cap. Oscillated samples are cylindrical, 10 mm in length and 2 to 10.3 mm in diameter. They are first inserted into an aluminum sample holder, which is then screwed onto the ruler. The sample holders are cylindrical capsules, 121 mm long with an outer diameter of 12 mm and inner dimensions of 101 mm length and a diameter ranging from 9.9 mm to 10.3 mm, ensuring proper sample centering. For samples with smaller diameters, such as gold rods, centering is achieved by replacing the holder's plugs with slightly longer plugs, partially drilled to match the dimensions of the samples. To ensure perfect alignment of the samples within the guide tube, the pulley used for the northern control rod is reused.



Fig. 2. The POLLEN pile-oscillator installed in the CROCUS zero-power reactor. On the left, motor, controller and wheel. The wire passes through the control rod pulley (on the top right) for precision guiding. The ruler connected to the wire is visible next to the double arrow that illustrates the linear displacement. The bottom of the ruler is inserted in the channel, with exiting optical fibers connected to miniature detectors set at the irradiation location.

The instrumented channel enables the measurement of local flux perturbations induced by sample insertion while maintaining its alignment during displacement. A picture of the channel instrumentation, ready for placement in the reactor core, is shown in Fig. 3.

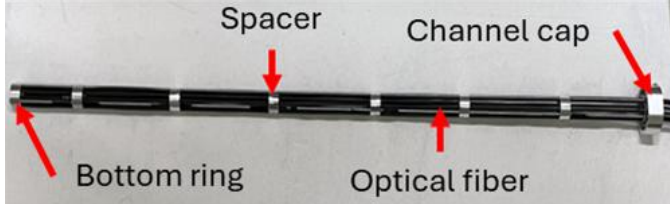


Fig. 3. Channel instrumentation ready to be placed in the north control rod guide tube. Six aluminum spacer ensure the sample alignment and straightness of the optical fibers

The instrumentation consists of an aluminum cap that fits onto the top of the control rod guide tube and a 20 mm long aluminum ring positioned at the core mid-height. The outer diameter of the ring matches the inner diameter of the guide tube, while its inner diameter is precisely manufactured to 12.2 mm to accommodate the sample holders. The ring is partially drilled with 12 holes: nine holes with a diameter of 2.2 mm accommodate miniature scintillators and their fibers, and three holes with a diameter of 2 mm serve as attachment points for three titanium structural rods. To enhance sample guidance, the 2-mm diameter holes protrude slightly toward the center of the ring, as shown in Fig. 4.

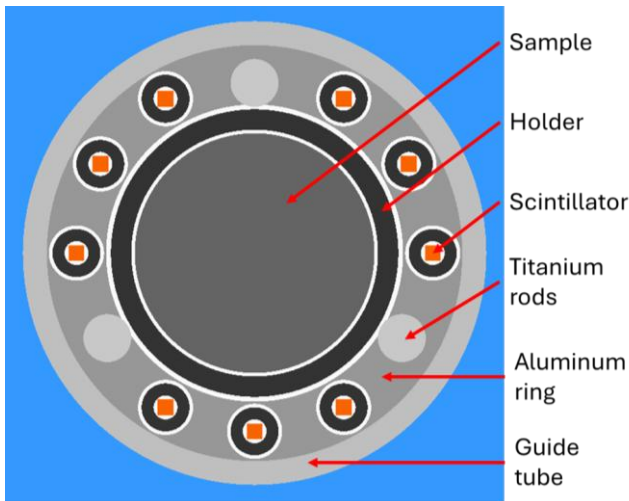


Fig. 4. Axial cross section of the instrumented channel at the reactor core mid-height, with a sample inserted. At the center is a sample encased in the sample holder. The three titanium rods, necessary for mechanical integrity, are visible in light gray. The nine orange squares are scintillators encased in their aluminum cap.

In addition to the titanium rods, the mechanical stability of the channel and the alignment of the fibers are guaranteed by six aluminum spacers, each 10 mm in length and visible in Fig. 3, into which the structural rods are embedded. The channel cap consists of two parts: a fixed component containing holes for the fibers, and a removable central plug that ensures the alignment of the sample holder and is unscrewed during sample exchange.

D. Analysis Methodology

The reactor time-dependent reactivity is calculated using inverse point kinetic, as was employed in the MAESTRO program [10,24,25]. The time-dependent reactivity $\rho_s(t)$ is obtained using (1) where $S_d(t)$, the delayed neutron source normalized to the reactor's normalized global signal $S_G(t)$, is computed using (2).

$$\rho_s(t) = 1 - \frac{\Lambda S_d(t)}{\beta S_G(t)} \quad (1)$$

$$\begin{cases} S_d(t) = \sum_i \lambda_i c_i(t) \\ \frac{dc_i(t)}{dt} = \frac{\beta_i}{\Lambda} S_G(t) - \lambda_i c_i(t) \end{cases} \quad (2)$$

With Λ the generation time, β the total delayed neutron fraction, c_i the i -th delayed neutron group normalized precursor concentrations, and the λ_i and β_i the respective decay constants and delayed neutron fractions.

The pseudo-square oscillation of the sample produces a corresponding pseudo-square signal in the time-dependent reactivity [9]. As the Fourier series representation of a square wave with amplitude 1 and period L is (3) [26].

$$S(x) = \frac{4}{\pi} \sum_{i=0}^{\infty} \frac{1}{2i+1} \sin\left(\frac{(2i+1)2\pi x}{L}\right) \quad (3)$$

The reactivity worth $\Delta\rho$ of the sample is measured as the full amplitude of the reactivity signal resulting from the pseudo-square oscillation. Its value is obtained by extracting the first harmonic of the time-dependent reactivity's Fourier transform $\tilde{\rho}$, as shown in (4).

$$\Delta\rho = \frac{\pi}{2} \|\tilde{\rho}(f_0)\| \quad (4)$$

Both the global and local signals, $S_G(t)$ and $S_L(t)$, are normalized by dividing each by its moving average over a window of length equal to their period T , similarly to the processing performed for during CORTEX [16]. The local perturbation $L(t)$ is then directly computed as the subtracting the global signal from the local signal [1,9,10].

$$L(t) = S_L(t) - S_G(t) \quad (5)$$

The quantities of interest – the global perturbation ΔG and the local perturbation ΔL – are defined as the amplitude of the first harmonic of $S_G(t)$ and $L(t)$ respectively. To estimate the uncertainties associated with these quantities and $\Delta\rho$, calculations are performed not on the full signal but on individual segments, each of two periods in length. The resulting set of estimates is then bootstrapped to obtain both the mean value of each quantity through the periods and the associated standard deviation [27].

Validation of the applicability of the point-kinetic assumption is performed by measuring the spectral power ratio (*SPR*) between each SAFFRON detector and one of its furthest detectors. The *SPR*, defined in (6) as the ratio between two detectors' normalized signals power, P_i and P_{ref} , is computed using the method (7) developed for the CORTEX program [15,16]. It allows comparing the relative noise distribution in a set of detectors. This method relies on cross-power spectral densities (CPSDs) with intermediate detectors j , yielding

estimates $P_{i,j}$, rather than direct pairwise computations. This approach produces a set of estimates from which the variance can also be evaluated. In the absence of spatial effects, all normalized signals are expected to exhibit the same power. Consequently, the spectral power ratio (SPR) would be equal to one.

$$SPR_{i,ref} = \frac{\sqrt{P_i}}{\sqrt{P_{ref}}} \quad (6)$$

$$SPR_{i,ref} = \frac{\sqrt{P_{i,i}}}{\sqrt{P_{ref,ref}}} = \frac{1}{n} \sum_j^n \frac{\sqrt{P_{i,j}}}{\sqrt{P_{j,ref}}} \quad (7)$$

Instead of computing a simple average, weights can be applied in (7) to account difference in detector performance. In BLOOM, the chosen weighting scheme uses the total number of counts recorded by the intermediate detector j over the full experiment as its weight in the calculation of the average and standard deviation.

III. RESULTS AND DISCUSSIONS

A. Point kinetic assumption verification

Verification of the absence of spatial effects in the core is carried out using signals measured during standard pile-oscillation experiments. The displacement follows a pseudo-square oscillation pattern, with a dwell time of 30 seconds at both the inserted and extracted positions, and a transition time of 2.4 seconds. In the inserted position, the center of the sample aligns with the mid-height of the core, placing it on the same horizontal plane as the SAFFRON L2 detectors and the scintillation detectors of the instrumented channel. The oscillation sequence consists of 84 periods, resulting in a total duration of slightly over an hour and a half. The reference detector for spectral power ratio calculations is the furthest mid-plane detector in SAFFRON, i.e., detector number 96 [13]. This choice is motivated by its distance from local flux perturbations caused by the sample, and by the higher count rate at the core mid-plane, which benefits from being the maximum of the cosine shaped axial flux distribution. The graph in Fig. 5 displays the results obtained with the largest gold sample used during the experimental campaign. The SPR values are plotted as a function of the distance from the perturbation and are grouped according to the respective detector plane.

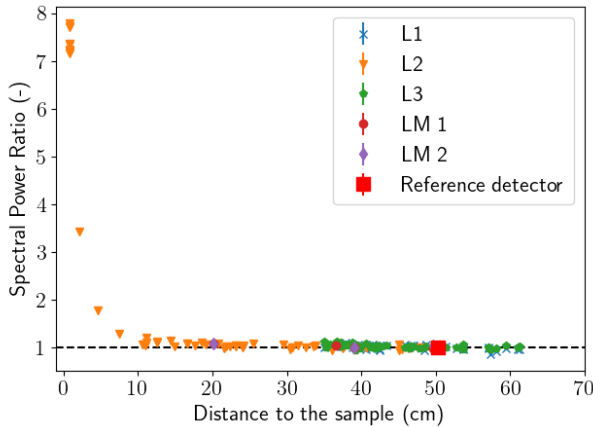


Fig. 5. Spectral Power Ratio (SPR) between each of the 160 detectors of SAFFRON and one at the opposite of the perturbation. The results are displayed as a function of the distance to the sample and grouped by the SAFFRON plane they are part of.

The results show that the local flux perturbation vanishes at a distance of 15 cm. Beyond this distance, all detectors have an SPR of 1 with respect to the reference detector, confirming that these detectors have the same modulation amplitude. It can therefore be concluded that, despite the local perturbation extending to 15 cm, the reactor continues to behave consistently accordingly to the point-kinetics model. This verification is essential for the experimental program, as variations in the spectral power ratios would indicate that the observed changes in detector count rates are partially caused by spatial redistribution of the neutron flux. In such a case, correction factors would be required to accurately retrieve the reactivity and global effect values. From these results it can be concluded that all detectors farther than 15 cm from the sample are suitable for the estimation of global perturbation.

B. Gold Sample Reactivity worth Measurements

The reactivity worth of the gold sample was measured five times between September 2024 and April 2025. The oscillation protocol was identical to that used for verifying the point-kinetics assumption: 84 pseudo-square periods, with a 30-second dwell time at each position and 2.4 seconds for each transition. Between each experiment, the sample holder was removed from the experimental channel, and the sample from the holder, while the oscillator remained untouched. Gold was chosen to perform repetitions because it is a standard in neutron activation dosimetry, and is also typically used to perform for power calibrations [20]. This makes it suitable for validating the implemented analysis methodology.

For each experiment, the time-dependent reactivity of the reactor is computed from the acquired signal using (1), the reactivity worth is then estimated using (5). The obtained values are shown in Fig. 6, alongside the reactivity worth computed through Monte Carlo simulation with the Serpent2 [28] neutron transport code and the JEFF-3.3 [29] nuclear data library.

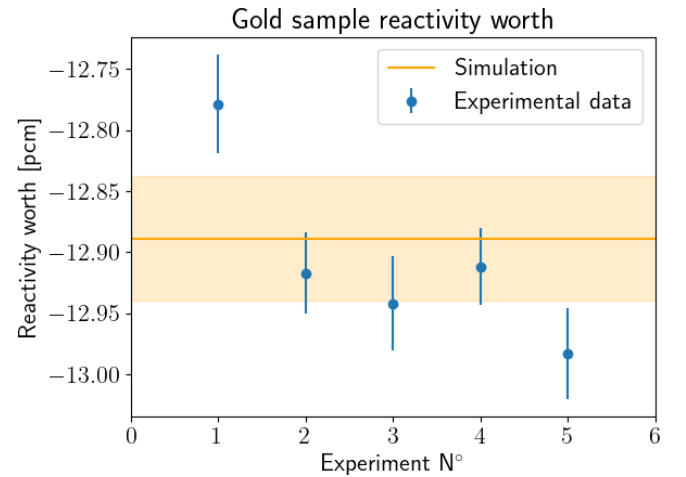


Fig. 6. Measured reactivity worth of a gold sample during five different experiments, performed between fall 2024 and spring 2025, and computed value with the Serpent2 MC code. All displayed uncertainties are 1 standard deviation.

The estimated experimental uncertainties range from 0.04 pcm to 0.05 pcm, corresponding to relative uncertainties

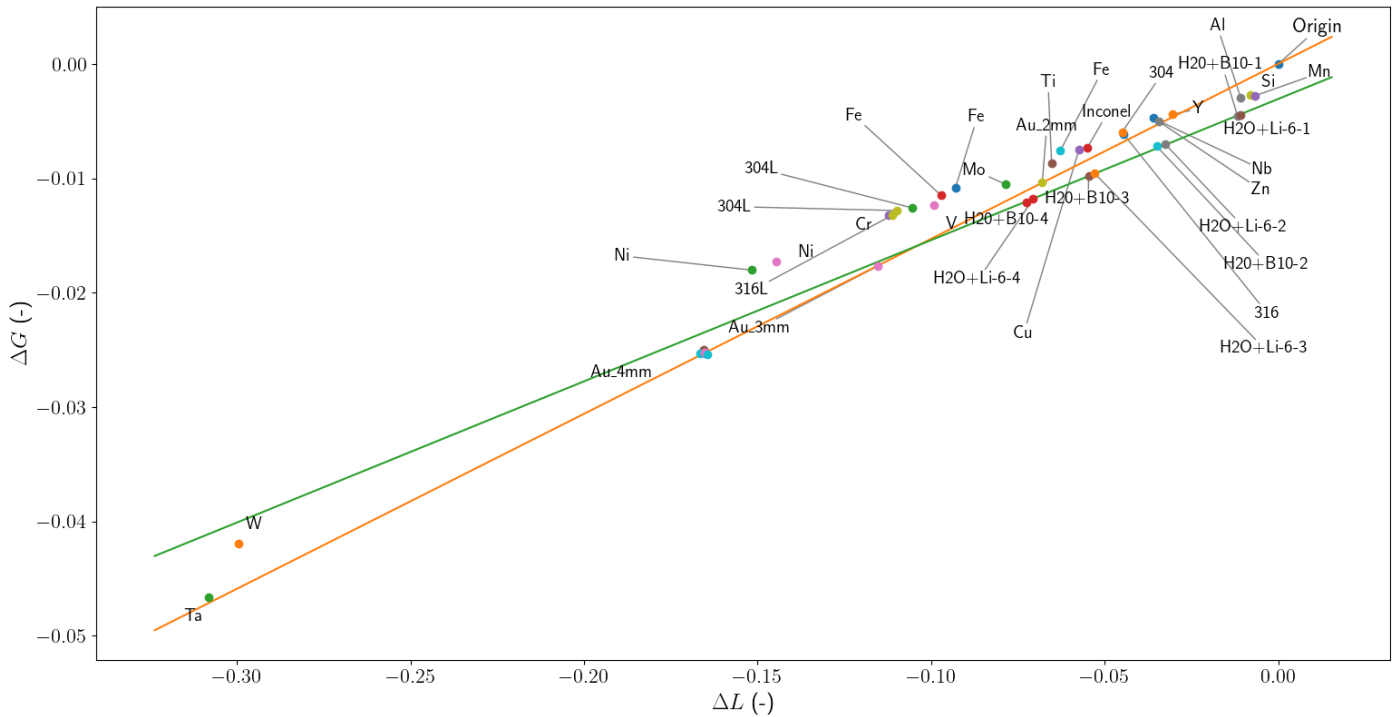


Fig. 7. Measured amplitude of the global signal ΔG vs. measured amplitude of the local perturbation ΔL for 40 experiments of the BLOOM program. Two linear regressions are also displayed: one for the measurement of gold samples with different diameters and one for the water samples with different neutron absorber concentrations.

on the order of 0.3%, as expected from the setup updates performed following the experimental design [1]. These variations are attributed to the differences in the average reactor power during the oscillations, which ranges from 800 mW to 950 mW, and to whether the power was stable or required correction for the drift in the power during the experiments due to a non-zero average of the reactivity during the oscillation. Although it is observed that the reactivity worth obtained during the measurement 1 may be an outlier, lying at more than two sigma from the experiments 3 and 5, the distance is not sufficient to rule the possibility of all of it being statistical. Moreover, the result from experiment 1 is supported by the simulations results, with which it agrees within two standard deviations. As shown in Fig. 6, all measurements are within two standard deviation agreements with the value obtained through Monte Carlo simulations, which has an uncertainty of the same order of magnitude as the experiments. This agreement support confidence in the implementation of the analysis methodology, which will later be applied to all samples in the experimental campaign.

C. Global and local effects

The BLOOM pile-oscillation program currently comprises a total of 45 oscillation experiments conducted on 40 different samples (25 different materials). All experiments follow the same protocol – 84 periods of pseudo-square pattern, with 30 seconds dwell times in each position and transition times of 2.4 seconds – defined to reach the targeted factor ten between measurement and nuclear data uncertainties for the iron sample [1]. The period averaged reactor power during oscillation was maintained constant at values varying between 800 mW and 950 mW.

Forty of the results are already analyzed and are shown in Fig. 7, using a layout commonly found in the literature and

especially the MAESTRO program, as the amplitude of the global signal ΔG against the amplitude of the local perturbation ΔL [9]. It is observed that the measurements globally align along a single axis in the graph, showing a qualitative proportionality between the decreases in ΔG the ΔL . This result was expected, as most samples act as additional thermal neutron absorbers in the core, inducing similar behaviors in core. The orientation of the axis itself is explained by the sensitivity of the detectors, used to measure the local perturbation, to thermal neutrons. The use of fast neutron sensitive detectors would yield different results. In terms of uncertainty, the global perturbation ΔG is consistent across the experiments, with values ranging between 8×10^{-5} and 1×10^{-4} . The estimated uncertainties show no significant dependence to the mean values, resulting in relative uncertainties ranging from 0.2% to 2%, depending on the sample's reactivity worth. Similarly, the uncertainty on the local perturbation ΔL shows no dependence on the mean value either. It ranges from the 1.4×10^{-4} to 1.8×10^{-4} , yielding large range of relative uncertainties that spans from 0.07% to 2.5% depending on the sample.

While the current measurement precision is sufficient for the study of stainless-steel main elements, with especially an experimental uncertainty on iron samples ten times smaller than the nuclear data induced one, as targeted [1]. Several options are available to reduce the uncertainties on the measurements of the global effects and reactivity worth of for low-effect samples. The simplest approach would be to increase the number of periods. However, this would reduce the uncertainty by a factor two at most, since reactor operations lasting more than six hours are unlikely and the uncertainties scales with the inverse of the square root of the number of fission, and thus of the oscillation time [5]. The second option is to increase the mass of the sample to increase the amplitudes of the

perturbations, as the uncertainty is observed to be independent of the amplitude. However, the limiting factor in this case is the size of the channel, which is already radially filled by most samples. Increasing the sample length is possible, but it would only affect the amplitude of the global perturbation. The last option is to increase the reactor power during pile-oscillations. Since uncertainty scales with inverse of the square root of the power, a factor 10 is theoretically achievable in the CROCUS reactor. However, the current limitation is the operational range of the detectors, which restricts the reactor power to 1 W. Operating the reactor at higher power in the future is feasible, but new instrumental developments and implementations are required.

Two linear regressions are also shown in Fig. 7. These are reproductions of two of the axes observed in the MAESTRO program, but obtained in the CROCUS reactor. The different linear trends observed in this type of graphs are hypothesized to be axes along which a macroscopic cross-section evolves. In this case it would be thermal neutron capture [9,30]. The first regression is the axis of the capture in water, and includes four ^{10}B in solutions (0.35 g/L, 0.69 g/L, 1.04 g/L, and 1.39 g/L) and four ^6Li solutions (0.82 g/L, 1.64 g/L, 2.46 g/L, and 3.28 g/L, each with 5% HNO_3). As shown in Fig. 8, the CROCUS measurements reproduce the expected linear trend, with a regression coefficient R^2 of 0.9993.

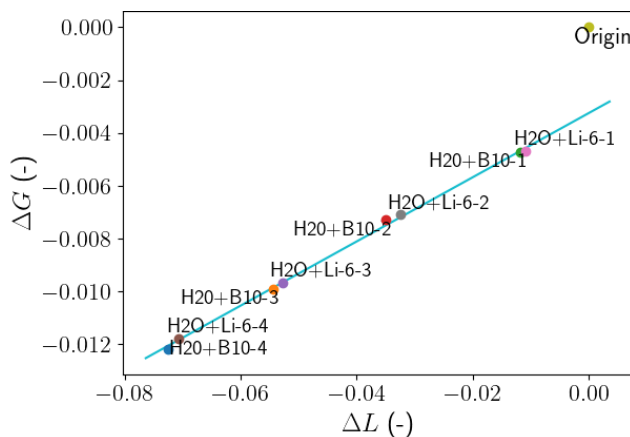


Fig. 8. Measured amplitude of the global signal ΔG vs. measured amplitude of the local perturbation ΔL for water samples of same volumes but with different absorber concentrations.

The second regression is based on the measurements using the gold samples. Three samples were measured, all of them long of 100 mm but with different radii of 4 mm, 3 mm, and 2 mm, respectively. The results are shown in Fig. 9. As with the water samples, the linearity is reproduced, with a regression coefficient R^2 of 0.9997. When extrapolated, the regression line passes near the origin of the coordinate system (i.e. unperturbed state), origin which was not part of the fitted data. In fact, it passes at a distance consistent with the previously mentioned uncertainties. This result is expected, as the linear trend in that direction corresponds to a decrease in mass up to an empty sample, i.e. sample with null radius, or, equivalently, to the total macroscopic cross-section moving toward zero. In contrast, for the water samples, only the capture cross-section changes significantly, so the regression line does not pass through the origin. These gold samples results provide additional

confidence in the quality of the measurements performed during the BLOOM program.

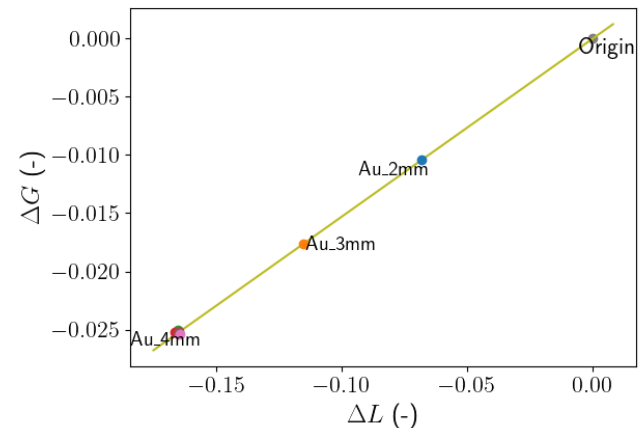


Fig. 9. Measured amplitude of the global signal ΔG vs. measured amplitude of the local perturbation ΔL for gold sample of different diameters. The origin is not included in the fitted data of the linear regression.

As mentioned previously (Sec. III.B), five repetitions were performed for the measurement of the gold sample with a diameter of 4 mm. Out of the five, only four measurements were used to perform the fit. The exclusion of the fifth point (experiment 2 in Fig. 6) is due to a difference in the sample holder used in this experiment compared to the others. In that experiment, the aluminum sample holder had an outer diameter of 12 mm, identical to the others, but an inner diameter 9.9 mm instead of the 10.3 mm used for the other samples. Thus, the holder was 0.2 mm thicker on both sides, which may affect the local perturbation ΔL measurements given the closeness of the local detectors. A close-up of these measurements, shown in Fig. 10, confirms this hypothesis. While the four measurements on the right of the graph form a consistent group, the measurement with the thicker holder (on the left) is at nine standard deviations from the average of the other four in the estimation of the local perturbation. These results demonstrate that the system is sensitive enough to detect such small differences in the measurement of the local perturbation ΔL , which, on the other hand, are not observable in the global effect ΔG .

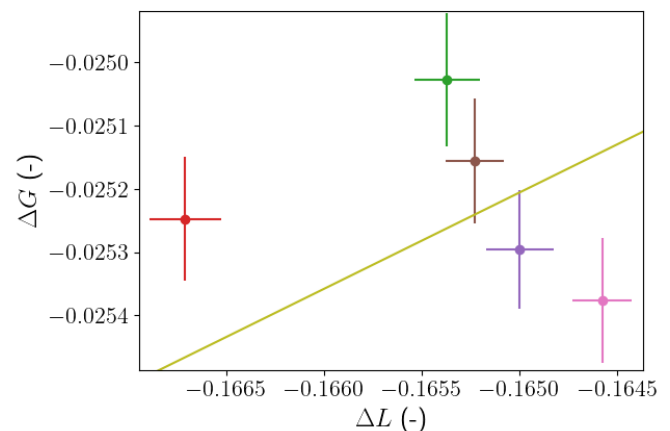


Fig. 10. Close-up on the repetitions of the measurement of the gold sample with a diameter of 4 mm. The measurement on the left side was performed with an aluminum holder thicker by 0.2 mm on both sides than the other four.

A pattern is observed in the distribution of the four measurements on the right side of in Fig. 10. All four are within two standard deviations from their average and are thus considered consistent with each other, but they also appear to be diagonally aligned. Although not yet studied, it is hypothesized that a negative correlation exists between the measurement uncertainties on the global and local effects. This may be expected, as the local perturbation over time, $L(t)$, is calculated using (5), which includes a subtraction of the global signal $S_G(t)$. These potential correlations for the gold samples, but also for all samples of the BLOOM program, will be investigated in future studies.

IV. CONCLUSION

The BLOOM pile-oscillation program was successfully conducted in the CROCUS reactor between fall 2024 and spring 2025. During the program, 45 oscillation experiments were carried out using 40 different samples and 25 materials, totaling over 200 hours of in-core experimentation.

As a first step, a gold cylinder with a reactivity worth 12.9 pcm, used as a reference, was oscillated and used to verify that the oscillation location was suitable for the program by checking that the flux distribution is only locally perturbed. It was observed that detectors located within 15 cm of the sample had perturbed count rates, while those farther away behaved as predicted by the point-kinetic model.

To validate the experimental and analysis methodologies, five repetitions of the gold sample oscillation experiment were performed to assess the consistency of the obtained reactivity worth. The results obtained show good agreement between themselves and with the value predicted by Monte Carlo simulations. Therefore, the implementation of the analysis methodology was validated and its robustness demonstrated.

The amplitudes of the local and global perturbations were successfully measured for each sample. The experimental uncertainties were found to show no dependence on the magnitude of the perturbations, with typically an uncertainty on the reactivity worth of 0.04 pcm. As a result, the relative uncertainty on local perturbations ranged from 2.5 % for the lightest sample to 0.07 % for the heaviest. Respectively, the uncertainty on global perturbations ranged from 2% to 0.2%. The experimental results reproduced the linear trends observed in the MAESTRO program for varying gold masses and neutron absorber concentration in water. The repetitions of the reference gold sample measurement showed that the experimental setup is sensitive enough to significantly measure the difference in local perturbation caused by a 0.2 mm variation in the thickness of the aluminum sample holder.

Next steps for the BLOOM pile-oscillation program in CROCUS include the addition of new reference samples such as D₂O. It also includes new instrumentation developments to be able to conduct new oscillations at higher power with the aim of decreasing the uncertainties on the measurements of low-reactivity samples. All results are to be included in a forthcoming NEA benchmark. Finally, new samples beyond structural materials are prospected for future pile-oscillation experiments in CROCUS.

AUTHORS CONTRIBUTIONS

Thomas Ligonnet designed and carried out the experiments, as well as performed the analysis and the redaction of this paper, as part of his PhD thesis.

Axel Laureau supervises Thomas Ligonnet's PhD thesis. He provided valuable feedback and help during the analysis.

Oskari Pakari is the CROCUS reactor installation chief. He contributed significantly to carrying out the experiments.

Daniel Clément participated in the design of the experimental channel and performed the mechanical production work.

Alexis Dupont-Bembinoff participated actively in the preparation of the experiments during the campaign.

Gilles Noguère provided feedback along the experimental program and enabled us to use samples from the MAESTRO program.

Andrea Pautz is Thomas Ligonnet's thesis director and the head of the LRS at EPFL.

Vincent Lamirand supervises Thomas Ligonnet's PhD thesis as co-director, and is in charge of LRS experimental research as Program manager. He is at the genesis of the experimental program and participated in the whole program.

ACKNOWLEDGMENT

The authors wish to thank Nicolas Weiss for the development of the pile-oscillator and Laurent Braun for his help with the electronics.

The authors also wish to thank Pierre Leconte and Benoît Geslot for their insight on the subject, and all people from CEA who took some of their time to enable us to use some of the MAESTRO program samples.

REFERENCES

- [1] T. Ligonnet et al., "Design of an Open-Loop Pile-Oscillation Program in the CROCUS Reactor," *IEEE Transactions on Nuclear Science* **71** 5, 1001 (2024); <https://doi.org/10.1109/TNS.2024.3371183>.
- [2] V. Lamirand, "Ten springs of experiments in CROCUS," *EPJ Web Conf.* **288**, 04026, EDP Sciences (2023); <https://doi.org/10.1051/epjconf/202328804026>.
- [3] V. Lamirand et al., "An Experimental Programme optimized with Uncertainty Propagation: PETALE in the CROCUS Reactor," *EPJ Web Conf.* **211**, O. Serot and A. Chebboubi, Eds., 03003 (2019); <https://doi.org/10.1051/epjconf/201921103003>.
- [4] A. Laureau et al., "Uncertainty propagation for the design study of the PETALE experimental programme in the CROCUS reactor," *EPJ Nuclear Sci. Technol.* **6**, 9, EDP Sciences (2020); <https://doi.org/10.1051/epjn/2020004>.
- [5] W. K. Foell, "Small-sample reactivity measurements in nuclear reactors," TID-26511, American Nuclear Society, Hinsdale, IL (1972).
- [6] B. A. Baker, "Comparison of open loop and closed loop reactivity measurement techniques on the ISU-AGN-201 reactor," Ph.D., Idaho State University (2013).
- [7] Y. Jiang et al., "Review of kinetic modulation experiments in low power nuclear reactors," *EPJ Nuclear Sci. Technol.* **6**, 55, EDP Sciences (2020); <https://doi.org/10.1051/epjn/2020017>.
- [8] D. Bernard, "Validation of actinides nuclear cross-section using pile-oscillation experiments performed at MINERVE facility," *Journal of the Korean Physical Society* **59** 2, 1119, Korea, Republic of (2011).

- [9] B. Geslot et al., “Innovative Hybrid Pile Oscillator Technique in the Minerve Reactor: Open Loop Versus Closed Loop,” *IEEE Transactions on Nuclear Science* **65** 11, 2767 (2018); <https://doi.org/10.1109/TNS.2018.2874690>.
- [10] B. Geslot et al., “A hybrid pile oscillator experiment in the Minerve reactor,” *Annals of Nuclear Energy* **108**, 268 (2017); <https://doi.org/10.1016/j.anucene.2017.04.036>.
- [11] V. Lamirand et al., “Analysis of the First COLIBRI Fuel Rods Oscillation Campaign in the CROCUS Reactor for the European Project CORTEX,” *EPJ Web Conf.* **247**, 21010, EDP Sciences (2021); <https://doi.org/10.1051/epjconf/202124721010>.
- [12] Y. Jiang et al., “PISTIL, a reactivity modulation device to probe the transfer function of the nuclear reactor CROCUS,” *EPJ Web Conf.* **253**, A. Lyoussi et al., Eds., 04007 (2021); <https://doi.org/10.1051/epjconf/202125304007>.
- [13] F. Vitullo, “Miniature and Minimalistic Neutron Detectors for Online High-Resolution Experiments in the Zero-Power Reactor CROCUS,” PhD thesis, EPFL (2022); <https://doi.org/10.5075/epfl-thesis-9492>.
- [14] F. Vitullo et al., “Design of a 150-miniature detectors 3D core-mapping system for the CROCUS reactor,” *EPJ Web Conf.* **253**, 04023, EDP Sciences (2021); <https://doi.org/10.1051/epjconf/202125304023>.
- [15] V. Lamirand et al., “CORTEX experiments – Part I: Modulation campaigns in AKR-2 & CROCUS for the validation of neutron noise codes,” *Annals of Nuclear Energy* **211**, 110928 (2025); <https://doi.org/10.1016/j.anucene.2024.110928>.
- [16] K. Ambrožič et al., “CORTEX experiments, Part II: Postprocessing of neutron noise time series to determine reliable mean and uncertainties,” *Annals of Nuclear Energy* **208**, 110704 (2024); <https://doi.org/10.1016/j.anucene.2024.110704>.
- [17] G. Noguere et al., “Interpretation of pile-oscillation measurements by the integral data assimilation technique,” *Nuclear Instruments and Methods in Physics Research Section A: Accelerators, Spectrometers, Detectors and Associated Equipment* **629** 1, 288 (2011); <https://doi.org/10.1016/j.nima.2010.11.034>.
- [18] A. Laureau et al., “Bayesian Monte Carlo assimilation for the PETALE experimental programme using inter-dosimeter correlation,” *EPJ Web Conf.* **239**, 18004, EDP Sciences (2020); <https://doi.org/10.1051/epjconf/202023918004>.
- [19] U. Kasemeyer et al., “Benchmark on Kinetic Parameters in the CROCUS Reactor,” 978-92-64-99020-3, Nuclear Energy Agency of the OECD (NEA), p. 93 (2007).
- [20] V. Lamirand et al., Eds., “Power calibration methodology at the CROCUS reactor,” *Advancements In Nuclear Instrumentation Measurement Methods And Their Applications (Animma 2019)*, E D P SCIENCES, Cedex A (2020); <https://doi.org/10.1051/epjconf/202022504022>.
- [21] O. Pakari et al., “Kinetic Parameter Measurements in the CROCUS Reactor Using Current Mode Instrumentation,” *IEEE Transactions on Nuclear Science* **65** 9, 2456 (2018); <https://doi.org/10.1109/TNS.2018.2831180>.
- [22] F. Vitullo et al., “A mm³ Fiber-Coupled Scintillator for In-Core Thermal Neutron Detection in CROCUS,” *IEEE Transactions on Nuclear Science* **67** 4, 625 (2020); <https://doi.org/10.1109/TNS.2020.2977530>.
- [23] T. Ligonnet et al., “POLLEN: A Pile-Oscillator for the BLOOM Experimental Program,” *EPJ Web Conf.* **288**, 04018, EDP Sciences (2023); <https://doi.org/10.1051/epjconf/202328804018>.
- [24] B. Geslot, C. Jammes, and B. Gall, “Influence of the delayed neutron group parameters on reactivity estimation by rod drop analysis,” *Annals of Nuclear Energy* **34** 8, 652 (2007); <https://doi.org/10.1016/j.anucene.2007.03.005>.
- [25] S. TAMURA, “Signal Fluctuation and Neutron Source in Inverse Kinetics Method for Reactivity Measurement in the Sub-critical Domain,” *Journal of Nuclear Science and Technology* **40** 3, 153, Taylor & Francis (2003); <https://doi.org/10.1080/18811248.2003.9715345>.
- [26] E. W. Weisstein, “Fourier Series--Square Wave;” <https://mathworld.wolfram.com/FourierSeriesSquareWave.html>; (current as of May 2, 2025).
- [27] B. Efron and R. J. Tibshirani, *An Introduction to the Bootstrap*, Chapman and Hall/CRC, New York (1994); <https://doi.org/10.1201/9780429246593>.
- [28] J. Leppänen et al., “The Serpent Monte Carlo code: Status, development and applications in 2013,” *Annals of Nuclear Energy* **82**, 142 (2015); <https://doi.org/10.1016/j.anucene.2014.08.024>.
- [29] A. J. M. Plompen et al., “The joint evaluated fission and fusion nuclear data library, JEFF-3.3,” *Eur. Phys. J. A* **56** 7, 181 (2020); <https://doi.org/10.1140/epja/s10050-020-00141-9>.
- [30] Y. Danon, “Innovative experiments for reduction of nuclear data uncertainty,” *EPJ Nuclear Sci. Technol.* **4**, 22, EDP Sciences (2018); <https://doi.org/10.1051/epjn/2018017>.